

# Journal Pre-proof

Studies of structural, magnetic and dielectric properties of X-type barium zinc hexaferrite  $\text{Ba}_2\text{Zn}_2\text{Fe}_{28}\text{O}_{46}$  powder prepared by combustion treatment method using *ginger* root extract as a green reducing agent

Amrin R. Kagdi, Robert C. Pullar, Sher Singh Meena, Rajshree B. Jotania, Khalid Mujasam Batoo

PII: S0925-8388(20)31483-3

DOI: <https://doi.org/10.1016/j.jallcom.2020.155120>

Reference: JALCOM 155120

To appear in: *Journal of Alloys and Compounds*

Received Date: 25 December 2019

Revised Date: 24 March 2020

Accepted Date: 8 April 2020

Please cite this article as: A.R. Kagdi, R.C. Pullar, S.S. Meena, R.B. Jotania, K. Mujasam Batoo, Studies of structural, magnetic and dielectric properties of X-type barium zinc hexaferrite  $\text{Ba}_2\text{Zn}_2\text{Fe}_{28}\text{O}_{46}$  powder prepared by combustion treatment method using *ginger* root extract as a green reducing agent, *Journal of Alloys and Compounds* (2020), doi: <https://doi.org/10.1016/j.jallcom.2020.155120>.

This is a PDF file of an article that has undergone enhancements after acceptance, such as the addition of a cover page and metadata, and formatting for readability, but it is not yet the definitive version of record. This version will undergo additional copyediting, typesetting and review before it is published in its final form, but we are providing this version to give early visibility of the article. Please note that, during the production process, errors may be discovered which could affect the content, and all legal disclaimers that apply to the journal pertain.

© 2020 Published by Elsevier B.V.



Credit Author statement

Amrin has prepared samples, prepared manuscript, data analysis, plotting graphs, FTIR and dielectric measurements, formal analysis, reply to reviewers, software

Robert C Pullar has checked manuscript fully, corrected, revised and time to time gave critical suggestions to improve the manuscript. English language and grammar are verified, conceptualization, visualization, funding acquisition

Sher Singh Meena has taken XRD, VSM, data analysis, revision and error analysis

Rajshree B. Jotania: supervision, methodology, writing- review and editing, investigation, data curation, administration

Khalid Mujasam Batoo: FE-SEM measurements, modify the draft including references, funding acquisition

All authors have read and agreed to the published version of the manuscript.

# Studies of structural, magnetic and dielectric properties of X-type Barium Zinc hexaferrite $\text{Ba}_2\text{Zn}_2\text{Fe}_{28}\text{O}_{46}$ powder prepared by combustion treatment method using *ginger* root extract as a green reducing agent

Amrin R. Kagdi<sup>a</sup>, Robert C. Pullar<sup>b</sup>, Sher Singh Meena<sup>c</sup>, Rajshree B. Jotania<sup>a,\*</sup>,  
Khalid Mujasam Batoo<sup>d</sup>

<sup>a</sup>Department of Physics, Electronics and Space Science, University School of sciences, Gujarat University, Ahmedabad – 380 009, Gujarat, India

<sup>b</sup>Department of Engineering of Materials and Ceramics/CICECO - Aveiro Institute of Materials, University of Aveiro, Aveiro 3810-193, Portugal

<sup>c</sup>Solid State Physics Division, Bhabha Atomic Research Centre, Mumbai 400 085, India

<sup>d</sup>King Abdullah Institute for Nanotechnology, King Saud University, Riyadh 11451, Saudi Arabia

\* Corresponding author, Email: rbjotania@gmail.com

## Abstract

Various quantities of *ginger* (*Zingiber officinale*) root extract were used to prepare X-type Barium-Zinc hexaferrite with the chemical composition  $\text{Ba}_2\text{Zn}_2\text{Fe}_{28}\text{O}_{46}$ . The powders were prepared using a combustion treatment method, being pre-heated at 550 °C for 4 h. with the *ginger* as a fuel, followed by final heating to 900 °C for 5 h. and natural cooling to room temperature to obtain  $\text{Ba}_2\text{Zn}_2\text{Fe}_{28}\text{O}_{46}$  hexagonal ferrite powder. The phase composition of heated powder samples was investigated by X-ray diffraction (XRD), indicating the formation of a mixture of X-type and hematite ( $\alpha\text{-Fe}_2\text{O}_3$ ). Up to 82.6 wt%, X-ferrite was formed at 900 °C with 52.5 g of *ginger* root extract. Dielectric analysis of the prepared samples shows the frequency-dependent phenomena. All samples were hard magnets, with coercivity values ( $H_C$ ) between 262.2-318.3 kA m<sup>-1</sup>, and squareness ratios > 0.5. The sample prepared with 52.5 g *ginger* root extract possesses the highest value of saturation magnetization ( $M_S = 33.87 \text{ Am}^2 \text{ kg}^{-1}$ ) in comparison with the other prepared samples. Therefore, *ginger* was shown to be a useful natural plant extract as a reducing fuel for the low-temperature synthesis of X-ferrites. The sample prepared with 35 g *ginger* root extract shows a broad resonance peak between 10 kHz to 100 kHz, while other samples show resonance between 500 kHz to 1 MHz frequency range. At low frequencies (100 Hz to 2 MHz), relative permittivity was constant between 5 and 12 above 800 kHz for all X- ferrites.

Keywords: Green synthesis, X-type hexaferrite, *ginger* root extract, magnetic properties, and dielectric properties.

## 1. Introduction

Currently, sustainable fresh approaches that use green chemistry to improve and protect our environment are the main concerns in many areas of research. Preparation of novel magnetic materials has become very attractive due to their potential applications in radar absorbing materials (RAM), electronics [1, 2], high-density magnetic recording [3-6], biocompatible magnetic nanoparticles for cancer treatment [7-10] and magnetic resonance imaging (MRI) [11, 12]. The development of biodegradable and cost-efficient synthesis methods of nanomaterial remains a scientific challenge. Nanotechnology is also important to defeat the environmental issues caused by chemical industries such as oils [13], organic dyes [14], mercury, and wastewater. Common nanoparticle synthesis using chemical methods often involves harmful chemicals and solvents which may affect the human body and environment. Hence, biological methods using natural plants or plant extracts for the preparation of nanoparticles can be used as important substitutes for chemical methods [15-18].

There are a large number of methods used for the synthesis of nanoparticles such as co-precipitation [19], sol-gel [20, 21], microemulsion [22] and standard ceramic methods [23, 24], but these methods are often not environmentally friendly as reagents and solvents used in these chemical processes can be flammable or toxic. To overcome this, green synthesis of nanoparticles using eco-friendly materials like plant extracts [25], microorganisms such as fungi, yeast [26] and bacteria [27] is a low cost, and time reducing alternative. Different plants, roots, leaves, fruits, fruit peel, seeds, and their extracts have been used for the preparation of magnetic nanomaterials [25, 28-30].

*Ginger* (*Zingiber officinale*) is a flowering plant and its root; rhizome is used as a spice [31]. An active constitute called gingerol in it is responsible for most of the health benefits from ginger [32]. *Ginger* is the world's most cultivated herb from its origin to the present having good historic and medicinal value as a digestive aid, aphrodisiac, etc., over thousands of years [33]. *Ginger* remains an important ingredient of many traditional herbal remedies, as it has a history of multiple uses [34]. Many anti-inflammatory and antioxidant compounds such as capsaicin, beta-carotene, pantothenic acid, curcumin, caffeic acid, and salicylate are present in it. Also, active compounds like

shogaol, zerumbone, terpenoids, flavonoids, paradol, and zingerone present in ginger provide many health benefits [35].

*Ginger* can be used as a reducing agent for the preparation of nanomaterials as it possesses good antioxidant properties [36, 37, 38]. It has been reported that antioxidant properties are associated with the reducing power of biologically active compounds [39, 40], useful during combustion synthesis.

Antioxidant activity and components vary greatly and depend on the extracting solvent and its concentration [41]. ~~In this work, we used water to produce *ginger* root extract, adding to the sustainability of the process.~~ In comparison with other work, our approach is an appropriate, inexpensive, time reducing and eco-friendly route for the green synthesis of barium-zinc X-type hexaferrite. This procedure is easier compared to earlier reported, being prepared from metal nitrates in water. To the best of our knowledge, it is the first time that barium-zinc hexaferrite (along with some hematite) has been formed at 900 °C by using *ginger* extract as a reducing agent in reactions.

In the present study, we have used different weights of *ginger* root to prepare X-type hexaferrites ( $\text{Ba}_2\text{Zn}_2\text{Fe}_{28}\text{O}_{46}$ ) by combustion treatment method and investigated the effect of the different amounts of ginger root on phase formation, as well as on magnetic and dielectric properties.

## 2. Experimental Procedure

### 2.1 *Ginger* extract preparation

Fresh *ginger* root (~ 200 g) was taken from the market and cleaned with distilled water. The *ginger* root was first peeled before cutting and then boiled for 45 minutes in 200 ml distilled water to get *ginger* root extract. The resulting extract solution was filtered using a filter paper.

### 2.2 X-type ferrite synthesis

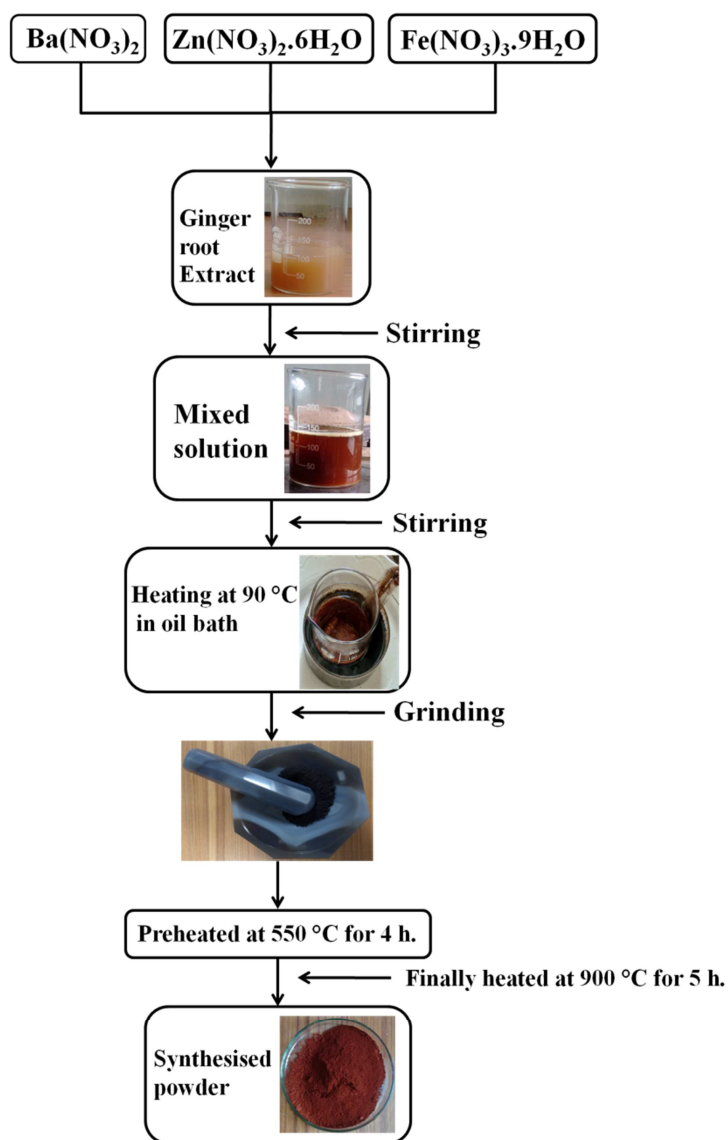


**Fig. 1.** Flowchart for the preparation of X-type hexaferrite  $\text{Ba}_2\text{Zn}_2\text{Fe}_{28}\text{O}_{46}$  powder.

Stoichiometric quantities of barium nitrate  $\text{Ba}(\text{NO}_3)_2$  ( $\geq 99.0\%$  pure, Sigma–Aldrich), zinc nitrate  $\text{Zn}(\text{NO}_3)_2 \cdot 6\text{H}_2\text{O}$  ( $\geq 98.0\%$  pure, Sigma–Aldrich) and ferric nitrate  $\text{Fe}(\text{NO}_3)_3 \cdot 9\text{H}_2\text{O}$  ( $\geq 98.0\%$ , pure, Sigma–Aldrich) were dissolved one by one in a total solution of 100 ml of *ginger* extract. Precursor solutions were made with 0.0, 17.5, 35.0, 52.5, and 70.0 g of *ginger* root and in all cases a total of 51.79 g of metal salts were added. During this process, the solution was continuously stirred using a magnetic stirrer. The prepared mixture was heated at  $90\text{ }^\circ\text{C}$  in an oil bath to obtain a gel. The obtained gel was then dried in a muffle furnace at  $100\text{ }^\circ\text{C}$  for 20 h., to remove water. The resulting dried powder was ground in a mortar and pestle and then preheated at  $550\text{ }^\circ\text{C}$  for 4 h. The preheated powder was finally heated to  $900\text{ }^\circ\text{C}$  for 5 h., in a muffle furnace and allowed to cool naturally to room temperature to obtain

the  $\text{Ba}_2\text{Zn}_2\text{Fe}_{28}\text{O}_{46}$  hexaferrite powder. Fig.1 shows the flowchart for the preparation of the X-type hexaferrite  $\text{Ba}_2\text{Zn}_2\text{Fe}_{28}\text{O}_{46}$  powder. Heated samples were coded as Sample (A), Sample (B), Sample (C), Sample (D) and Sample (E) for the  $\text{Ba}_2\text{Zn}_2\text{Fe}_{28}\text{O}_{46}$  hexaferrite prepared with 17.5, 35.0, 52.5, 70.0 and 0.0 g of *ginger* root extract, respectively.

### 2.3 Characterisation

A FTIR spectrometer (Bruker Tensor 27 Model) was used to record infrared (IR) spectra of all synthesised samples over the range of  $4000\text{--}400\text{ cm}^{-1}$  at room temperature. KBr pellet method was used to record IR spectra. X-ray diffraction (XRD) technique was used to identify the crystalline phase formation, using a Rigaku X-ray diffractometer with  $\text{Cu - K}\alpha$  radiation ( $\lambda = 1.5406\text{ \AA}$ ), and the  $2\theta$  scanning range was  $20^\circ\text{--}80^\circ$  with equal steps of  $0.02^\circ$ . The morphology of all samples was investigated using a Nano Nova 450 Field Emission Gun Scanning Electron Microscope (FEG-SEM). The magnetic hysteresis loops were recorded at room temperature under an applied field of  $\pm 1.0\text{ T}$  using a vibrating sample magnetometer (EG & G Princeton Applied Research instrument, Model 4500) The low-frequency dielectric measurements were carried out at room temperature over a frequency range of 100 Hz to 2 MHz using a Precision LCR meter (Agilent E4980A). The pellets of sintered ferrite powder were made using a hydraulic press for low-frequency dielectric measurements and density measurements.

## 3. Results and discussions

### 3.1 FTIR Analysis

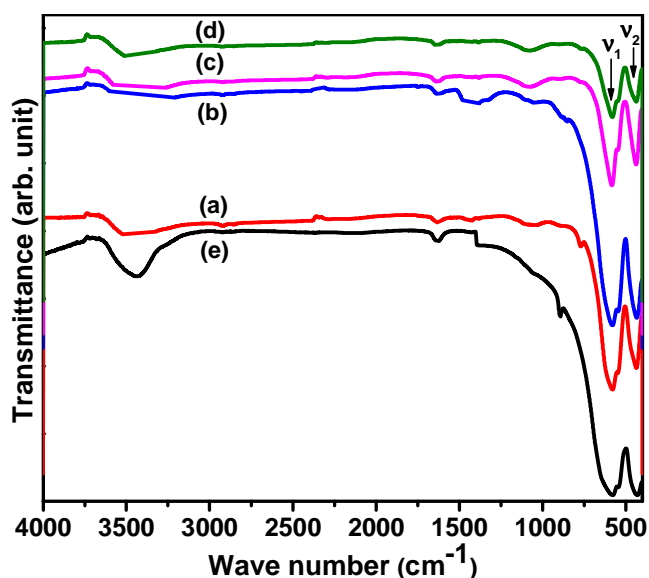


**Fig. 2.** FTIR spectra of X-type  $\text{Ba}_2\text{Zn}_2\text{Fe}_{28}\text{O}_{46}$  hexaferrite samples heated at  $900\text{ }^\circ\text{C}$  for 5 h., prepared with and without the presence of different weight ratios of *ginger* root extract: (a) Sample (A), (b) Sample (B), (c) Sample (C), (d) Sample (D), and (e) Sample (E).

Fig. 2 shows the FTIR spectra of  $\text{Ba}_2\text{Zn}_2\text{Fe}_{28}\text{O}_{46}$  powder synthesised with and without the presence of *ginger* root extract heated at  $900\text{ }^\circ\text{C}$  for 5 h (Sample (A-E)). The absorption bands in the powder at  $584\text{ cm}^{-1}$  and  $434\text{ cm}^{-1}$  are assigned to the tetrahedral ( $\nu_1$ ) and octahedral ( $\nu_2$ ) metal-oxygen bond vibrations of the crystal lattice, and are characteristic of hexagonal ferrites [42]. Absorption bands in the range  $434\text{-}439\text{ cm}^{-1}$  ( $\nu_2$ ) are assigned to the Fe-O stretching of  $\text{Fe-O}_6$ , while, the bands in the range  $580\text{-}585\text{ cm}^{-1}$  ( $\nu_1$ ) are assigned to the Fe-O stretching of  $\text{Fe-O}_4$  [43]. All heated samples show a small absorption band at  $\sim 1632\text{ cm}^{-1}$ , indicating the O-H stretching vibrations which may be due to the polyol [44]. However, the sample prepared without *ginger* root extract shows a broad (strong) absorption peak between  $3300\text{-}3600\text{ cm}^{-1}$ , which is due to the stretching vibration of an O-H bond [45, 46], and is typical of water. The fact that this is absent in the samples with *ginger* suggests that the sample without *ginger* (Sample (E), Fig. 2e) is much more hygroscopic and has absorbed atmospheric moisture much more rapidly after cooling.

### 3.2 XRD analysis

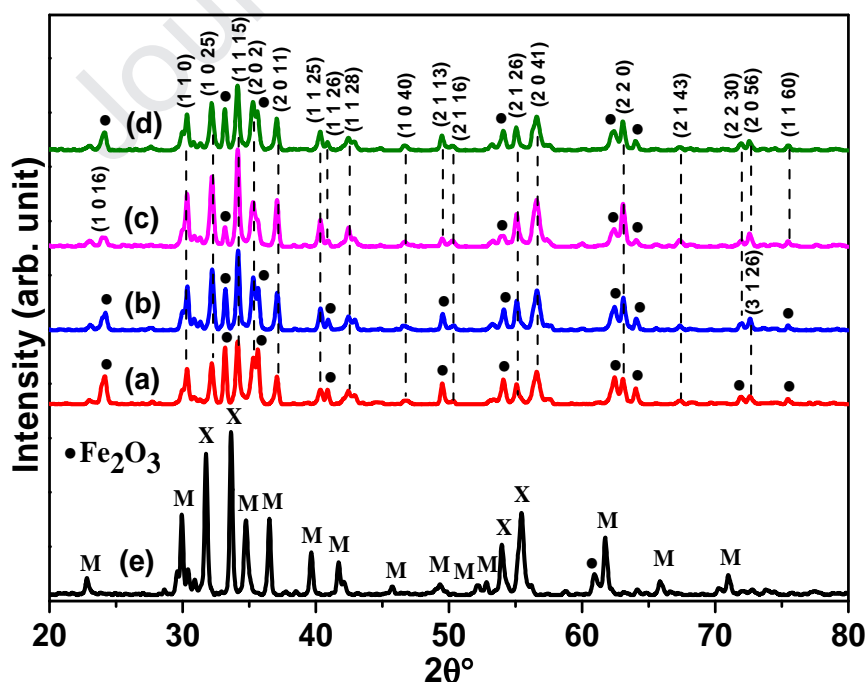




**Fig. 3.** XRD patterns of X-type  $\text{Ba}_2\text{Zn}_2\text{Fe}_{28}\text{O}_{46}$  hexaferrite samples heated at 900 °C for 5 h., prepared with and without the presence of different weight ratios of *ginger* root extract: (a) Sample (A), (b) Sample (B), (c) Sample (C), (d) Sample (D), and (e) Sample (E).

XRD patterns of X-type  $\text{Ba}_2\text{Zn}_2\text{Fe}_{28}\text{O}_{46}$  hexaferrite samples were indexed using the standard patterns for X-type ( $\text{Ba}_2\text{Me}_2\text{Fe}_{28}\text{O}_{46}$ ) hexagonal crystals (JCPDS # 01-073-2034), and are shown in Fig. 3. XRD analysis of the samples, prepared in the presence of different weight ratios of *ginger* root extract and heated at 900 °C for 5 h. revealed the formation of X-type ferrite and hematite ( $\alpha\text{-Fe}_2\text{O}_3$ ) (JCPDS # 04-015-9569) as a minor secondary phase. However, the sample prepared without *ginger* root extract (Sample (E)) shows the formation of a mixture of phases: 72.2% of M-type ferrite ( $\text{BaFe}_{12}\text{O}_{19}$ ) (JCPDS # 84-0757), only 22.2% X-type, and 5.6% hematite. Therefore, the addition of the *ginger* extract has enabled the formation of a single hexaferrite phase (X-type) at a low temperature of only 900 °C, with non-magnetic  $\alpha\text{-Fe}_2\text{O}_3$  as a minor secondary phase. The phase composition values are given in Table 1.

It can be seen from Fig. 3 that the sample with 52.5 g weight of *ginger* root extract (Sample (C), Fig. 3c) contained the lowest amount of hematite compared to the others, with 82.61 % X ferrite, while the quantity of hematite increased again when the weight ratio of *ginger* root extract increased to 70 g (Sample (D), Fig. 3d), yielding 75.0 % X ferrite. Therefore, the XRD patterns confirmed that 52.5 g weight of *ginger* root extract (Sample (C), Fig. 3c) was the optimum for the synthesis of X-type ( $\text{Ba}_2\text{Zn}_2\text{Fe}_{28}\text{O}_{46}$ ) hexaferrites.

The variation of lattice constants and unit cell volume with different weight ratios of *ginger* root extract is shown in Fig. 4 and Table 1. The average crystallite size was investigated from the most intense peak using the following Scherrer formula [47].

$$D_{(xrd)} = \frac{K\lambda}{\beta \cos\theta} \quad (1)$$

Where  $K$  is a dimensionless shape factor and has a value about of 0.9 which varies with the actual shape of the crystallite;  $\lambda$  is the X-ray wavelength (1.5406 Å);  $\theta$  is the angle of Bragg diffraction, and  $\beta$  is the full width at half the maximum intensity. The obtained structural parameters are listed in Table 1. The crystallite size of all samples, heated at 900 °C for 5 h. varies in the range of 27-37 nm.

The unit cell volume was calculated using the following equation.

$$V = a^2c \sin 120^\circ \quad (2)$$

Where ‘ $V$ ’ is the volume of the unit cell and ‘ $a$ ’ and ‘ $c$ ’ are the lattice constants.

The crystallite size was  $\sim 37$  nm without *ginger* extract, and  $\sim 30$  nm in all cases with *ginger* extract, suggesting that the reducing agent had the effect of slightly lowering crystallite size in the ferrites produced. Similarly, the lattice parameters and cell volume were larger, and similar, for all samples produced with *ginger* extract compared to that without.

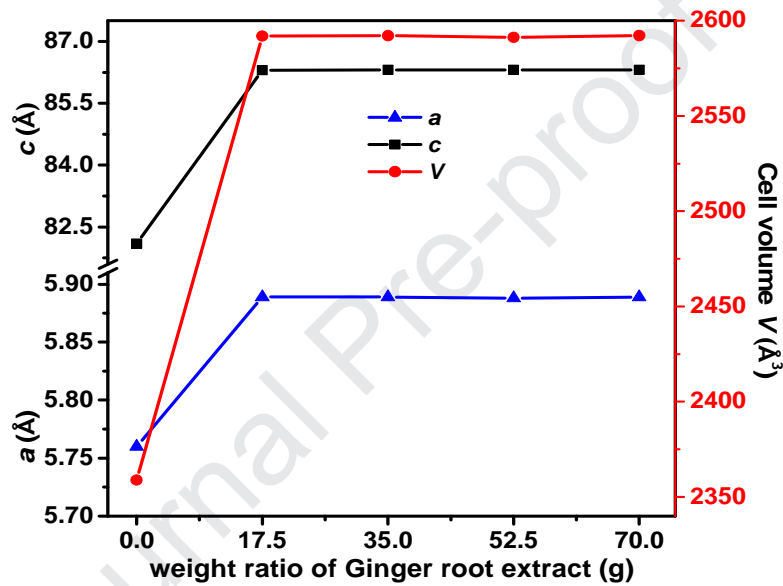


**Fig. 4.** Variation of Lattice constants ( $a$ ,  $c$ ) and unit cell volume ( $V$ ) of  $\text{Ba}_2\text{Zn}_2\text{Fe}_{28}\text{O}_{46}$  hexaferrite samples prepared without *ginger* root extract and with different weight ratios of *ginger* root extract heated at  $900^\circ\text{C}$  for 5 h. (Sample (A-D))

**Table 1.** Structural parameters of X-type  $\text{Ba}_2\text{Zn}_2\text{Fe}_{28}\text{O}_{46}$  hexaferrite samples prepared without and with the different weight ratio of *ginger* root extract and heated at  $900^\circ\text{C}$  for 5 h.

Code	Lattice parameters		Cell volume $V$ (Å <sup>3</sup> ) (±5)	Crystallites size $D_{\text{xrd}}$ (nm) (±0.2)	FWHM (deg.)	% of X-phase (±0.1)	% of $\alpha$ - $\text{Fe}_2\text{O}_3$ (±0.1)	% of M-phase (±0.1)
	$a$ (Å) (±0.02)	$c$ (Å) (±0.2)						
Sample (A)	5.889	86.303	2592.03	29.30	0.2964	58.33	41.67	-
Sample (B)	5.889	86.308	2592.18	31.34	0.2771	62.50	37.50	-
Sample (C)	5.888	86.310	2591.35	30.15	0.2880	82.61	17.39	-
Sample (D)	5.889	86.310	2592.24	27.91	0.3111	75.00	25.00	-
Sample (E)	5.760	82.10	2358.88	36.95	0.2350	22.22	5.56	72.22

The values of Bulk density ( $d_B$ ) and X-ray density ( $D_x$ ) were calculated using the following equations [48].

$$d_B = \frac{m}{\pi r^2 h} \quad (3)$$

$$D_x = \frac{3M}{Na^2c} \quad (4)$$

Where  $m$  is mass of pellet,  $r$  is a radius of pellet,  $h$  is the height (thickness) of pellet,  $M$  is molecular weight,  $a$  and  $c$  are lattice constants, and  $N$  is Avogadro's number ( $6.02 \times 10^{23}$ /mole).

The value of porosity for all samples is calculated using the following equation.

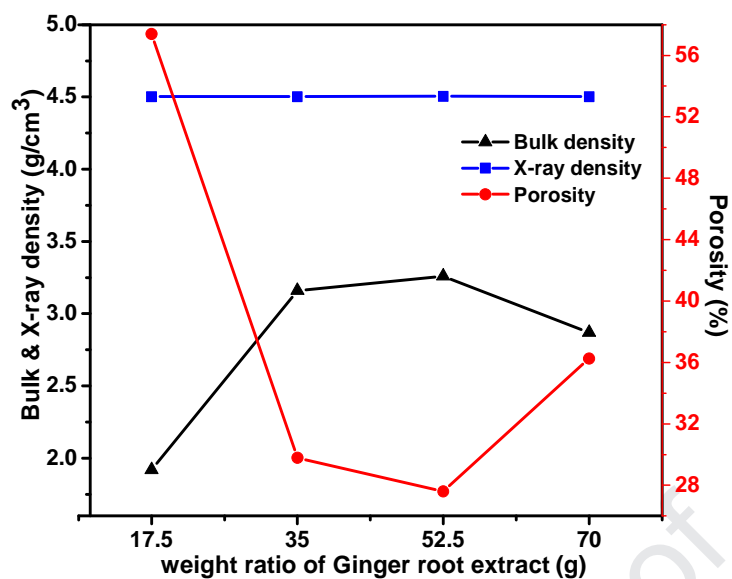
$$P = (1 - \frac{d_B}{D_x}) \times 100 \% \quad (5)$$

The calculated values of X-ray, bulk density and porosity of all the samples heated at 900 °C for 5 h. are shown in Table 2. The value of bulk density varies in the range of 1.90 - 3.30 g/cm<sup>3</sup> (Table 2). The sample prepared with 52.5 g *ginger* root extract (Fig. 3c), that contained the most X-ferrite phase, also had the minimum value of porosity and maximum value of bulk density. However, as these pellets were only heated to 900 °C, hence they are very poorly sintered and are not close to the maximum density possible (5.313 g/cm<sup>3</sup>). The calculated X-ray densities were higher, at ~ 4.50 g/cm<sup>3</sup> (see Table 2).

**Table 2.** The bulk density, X-ray density, and the porosity of Ba<sub>2</sub>Zn<sub>2</sub>Fe<sub>28</sub>O<sub>46</sub> hexaferrite samples heated at 900 °C for 5 h.

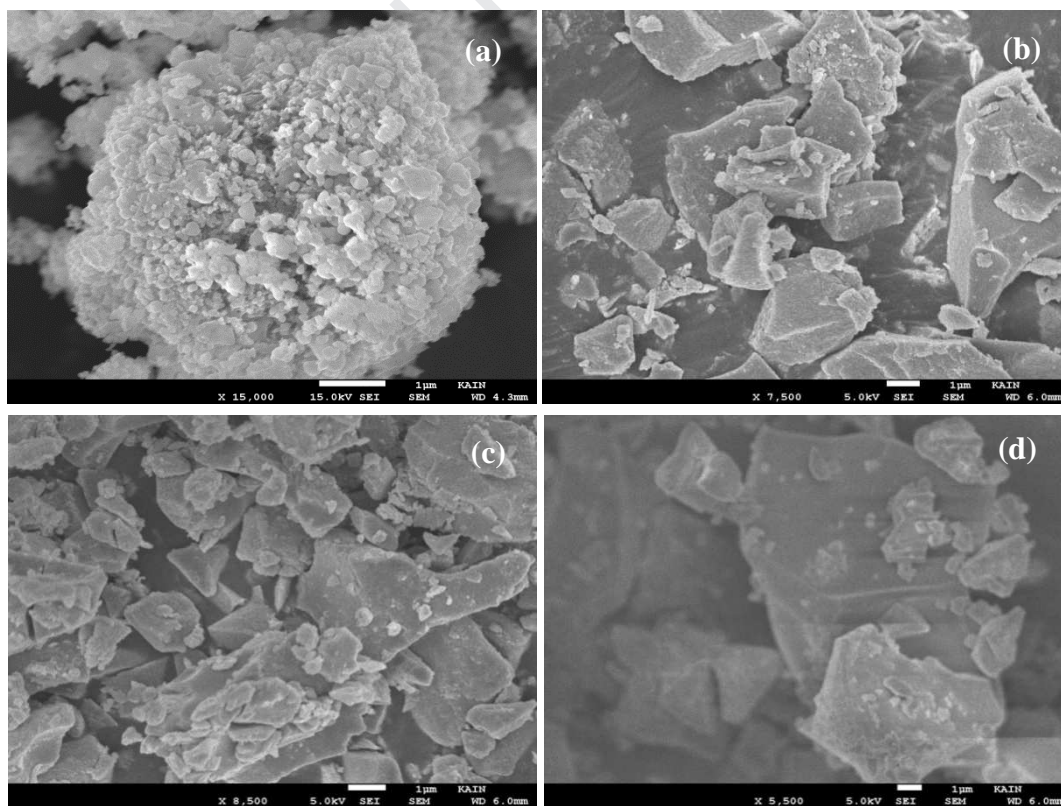
<b>Code</b>	<b>Bulk density <math>d_B</math> (g/cm<sup>3</sup>) (± 0.01)</b>	<b>X-ray density <math>D_x</math> (g/cm<sup>3</sup>) (± 0.02)</b>	<b>Porosity P (%) (± 0.1)</b>
Sample (A)	1.92	4.502	57.40
Sample (B)	3.16	4.502	29.79
Sample (C)	3.26	4.504	27.60
Sample (D)	2.87	4.502	36.25

Fig. 5 shows the variation in bulk density ( $d_B$ ), X-ray density ( $D_x$ ) and porosity ( $P$ ) with the different weight ratios of *ginger* root extract for the samples heated at 900 °C for 5 h.



**Fig. 5.** Variation of the Bulk density, X-ray density, and porosity of  $\text{Ba}_2\text{Zn}_2\text{Fe}_{28}\text{O}_{46}$  hexaferrite samples prepared with the different weight ratios of *ginger* root extract heated at 900 °C for 5 h. (Sample (A-D))

### 3.3 Surface Morphology



**Fig. 6.** SEM images of  $\text{Ba}_2\text{Zn}_2\text{Fe}_{28}\text{O}_{46}$  hexaferrite samples heated at 900 °C for 5 h., prepared with the presence of different weight ratios of *ginger* root extract: (a) Sample (A), (b) Sample (B), (c) Sample (C), (d) Sample (D).

Fig.6 shows the SEM micrographs for all the samples (Sample (A-D)) showing the grain morphology of prepared hexaferrites. It is observed from micrographs that the grains are agglomerated and are irregular in shape. As the weight ratio of *ginger* root extract increases, porosity decreases, and agglomeration increases. The sample prepared in presence of 17.5 g *ginger* root extract ( Sample (A), Fig. 6a) possesses spongy structure and it also possesses a high value of porosity (57.40 %) and low value of bulk density ( $1.92 \text{ g/cm}^3$ ) compared to all other samples.

### 3.4 Magnetic properties

The hysteresis loops of  $\text{Ba}_2\text{Zn}_2\text{Fe}_{28}\text{O}_{46}$  samples prepared in the presence of *ginger* root extract, heated at  $900 \text{ }^\circ\text{C}$  were recorded on a VSM under an applied field of  $\pm 1.0 \text{ T}$  and shown in Fig. 7. The different magnetic parameters such as saturation magnetisation ( $M_S$ ), remanent magnetisation ( $M_r$ ), coercivity ( $H_C$ ), and squareness ratio ( $M_r/M_S$ ) of prepared hexaferrites are calculated from the M-H loops and their values are listed in Table 3.

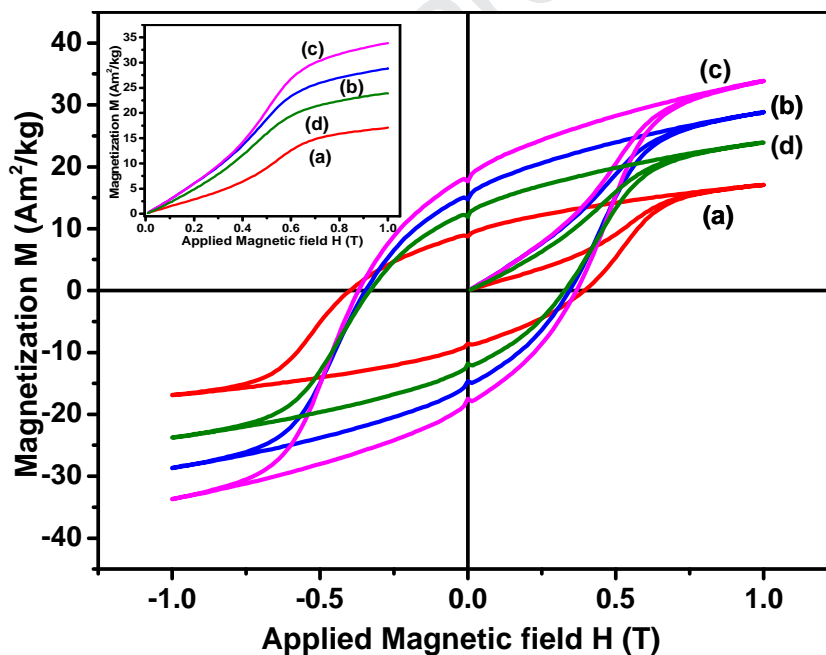


**Fig.7.** M-H loops and initial magnetization curves (inset) of  $\text{Ba}_2\text{Zn}_2\text{Fe}_{28}\text{O}_{46}$  hexaferrite samples heated at  $900 \text{ }^\circ\text{C}$  for 5 h., prepared with the different weight ratio of *ginger* root extract: (a) Sample (A), (b) Sample (B), (c) Sample (C), (d) Sample (D).

**Table 3.** Magnetic parameters of  $\text{Ba}_2\text{Zn}_2\text{Fe}_{28}\text{O}_{46}$  hexaferrites prepared with the different weight ratios of *ginger* root extract heated at  $900 \text{ }^\circ\text{C}$  for 5 h.

The values of saturation magnetisation ( $M_S$ ) and remanent magnetisation ( $M_r$ )

Sr. No.	Code	Remanence Magnetization $M_r$ ( $\text{Am}^2 \text{kg}^{-1}$ )	Saturation Magnetization $M_S$ ( $\text{Am}^2 \text{kg}^{-1}$ )	Squareness ratio $M_r/M_S$	Coercivity $H_C$ (T)	$H_a$ ( $\text{kA m}^{-1}$ )	$H_a$ (Oe)
1	Sample (A)	8.75	17.08	0.5122	0.40	149.71	1881.25
2	Sample (B)	14.75	28.86	0.5110	0.35	156.73	1969.47
3	Sample (C)	17.66	33.87	0.5214	0.38	147.17	1849.34
4	Sample (D)	11.92	20.92	0.5698	0.33	108.10	1358.38

increase as the weight ratio of *ginger* root extract increases except for the sample prepared with 70.0 g *ginger* root extract (Sample (D)), that had a lower X-ferrite content than that with 52.5 g, as shown in Table 3. The value of coercivity lies in the range of 262.6-318.3  $\text{kA m}^{-1}$  (0.33-0.40 T = 3300-4000 Oe) in all cases, which shows that the prepared samples belong to the family of hard ferrites [49], as would be expected for  $\text{Ba}_2\text{Zn}_2\text{Fe}_{28}\text{O}_{46}$ . The variation of saturation magnetisation ( $M_S$ ), remanent magnetisation ( $M_r$ ) and coercivity ( $H_C$ ) with the different weight ratios of *ginger* root extract are shown in Fig. 8 (a).

In the present study, the sample prepared with 52.5 g *ginger* root extract (Sample (C)) possesses the highest value of saturation magnetisation ( $M_S = 33.87 \text{ Am}^2 \text{kg}^{-1}$  or  $\text{emu/g}$ ) in comparison with the remaining prepared samples, that is because this sample exhibits the maximum amount of X-phase (79.16 %). The variation in  $M_S$  is matching with X-phase presented in the sample as shown in Fig. 8 (b). This  $M_S$  value ( $33.87 \text{ Am}^2 \text{kg}^{-1}$  or  $\text{emu/g}$ ) is particularly low in comparison with the reported maximum value of saturation magnetisation ( $M_S = 73.1 \text{ Am}^2 \text{kg}^{-1}$  or  $\text{emu/g}$ ) [50]. The low value of  $M_S$  is partially attributed to the presence of the antiferromagnetic phase of hematite (17.39 % of  $\alpha\text{-Fe}_2\text{O}_3$ ) [51, 52], as confirmed by XRD analysis (Fig. 3), as a sample containing only 82.61 wt % X ferrite would be expected to have a  $M_S$  value of  $57.75 \text{ Am}^2 \text{kg}^{-1}$ . The fact that the value here is still only around 2/3 of this value could be explained by the low synthesis temperature used here – magnetisation is known to increase as synthesis/sintering temperature increases, and the low crystallite size seen in these samples is well below the typical maximum magnetic domain sizes reported for hexaferrites of between 0.5-1  $\mu\text{m}$  [2]. The squareness ratio ( $M_r/M_S$ ) is also calculated from the values of  $M_r$  and  $M_S$  and their values are tabulated in Table 3. Previously, it has been reported that the squareness ratio of hexaferrite samples at or above 0.5 shows the material possesses a single magnetic domain and below 0.5 shows the formation of a multi-

domain structure. In the present study, the squareness ratio of all the samples is in the range of 0.510 - 0.570 (Table 3) showing that all the samples possess a single domain structure.

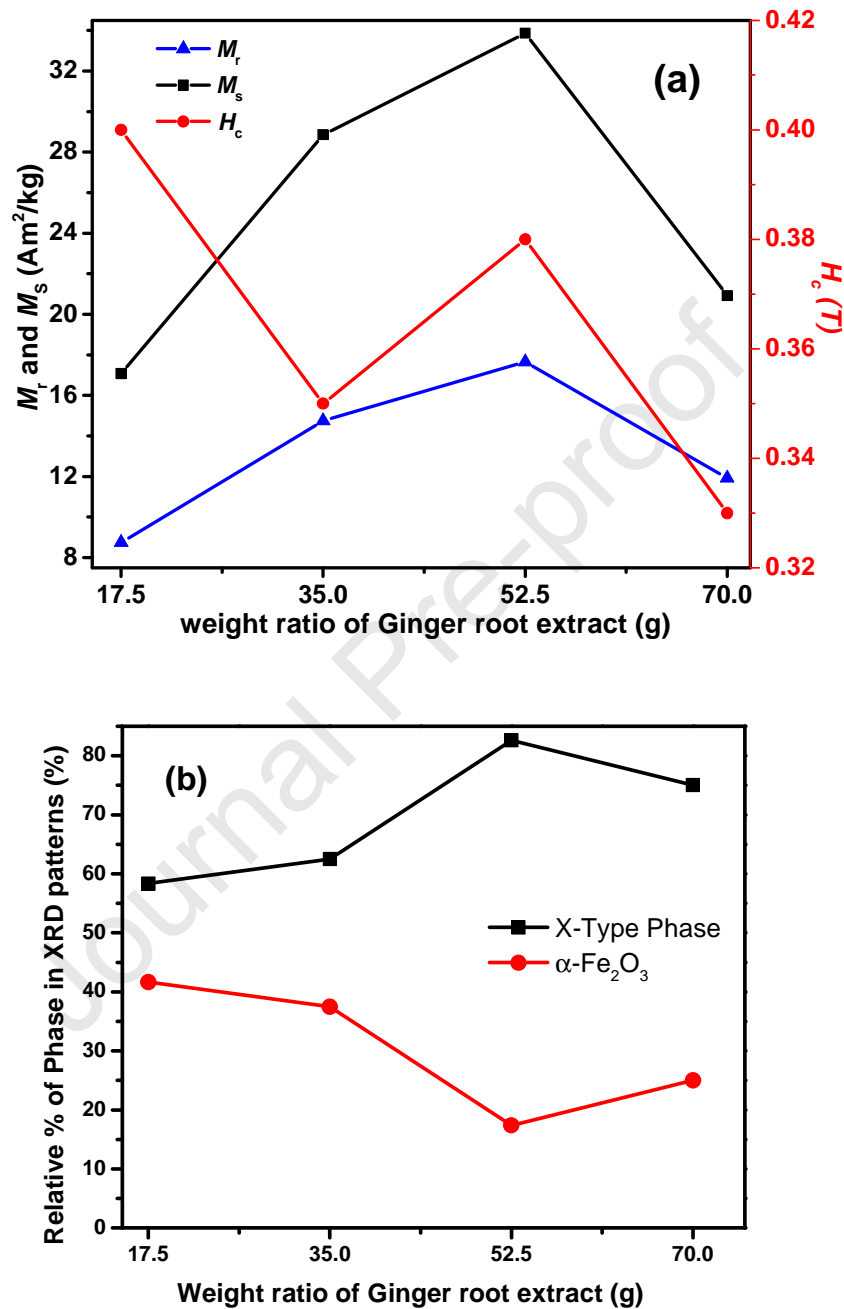


**Fig. 8.** (a) Variation in saturation magnetization ( $M_s$ ), remanent magnetization ( $M_r$ ), ( $H_c$ ), and, (b) Relative percentage of two phases of  $\text{Ba}_2\text{Zn}_2\text{Fe}_{28}\text{O}_{46}$  hexaferrite samples prepared with the different weight ratios of *ginger* root extract heated at  $900\text{ }^\circ\text{C}$  for 5 h. (Sample (A-D)).



### 3.5 Dielectric properties

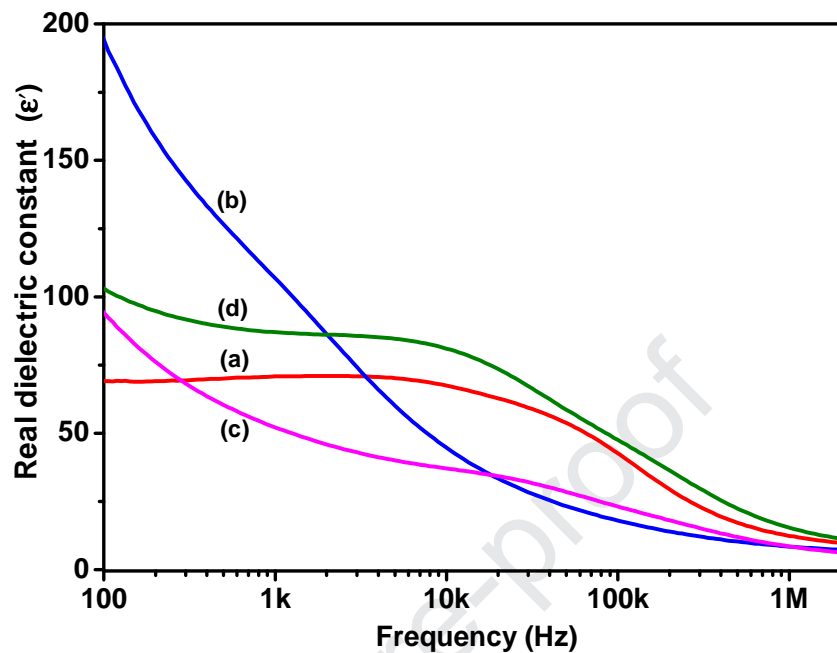


**Fig. 9.** Variation in real dielectric constant ( $\epsilon'$ ) of  $\text{Ba}_2\text{Zn}_2\text{Fe}_{28}\text{O}_{46}$  hexaferrite samples heated at  $900\text{ }^\circ\text{C}$  for 5 h., prepared with the different weight ratio of *ginger* root extract: (a) Sample (A), (b) Sample (B), (c) Sample (C), (d) Sample (D).

It is observed from Fig. 9 that at low-frequency, the dielectric constant of the samples prepared with 35 g *ginger* root extract (Sample (B)) decreases rapidly and approaches a constant above 1 MHz, while the other samples (Sample (A), (C) and (D)) show lower initial permittivity, and resonance peaks at around 10-50 kHz. This decrease in dielectric constant with frequency is a normal behaviour of most ferri-magnetic materials and has also been observed by several other researchers [53-55]. This behaviour of dielectric dispersion can be explained based on Koop's phenomenological theory, which is based on the Maxwell-Wagner interfacial polarisation model [56]. According to this model, the dielectric medium of ferrite consists of two layers. The first layer of fairly well-conducting boundaries is separated by the second layer of relatively poor conducting boundaries. The first layer is strongly effective at higher frequencies, while the second layer is dominant at lower frequencies. The free electrons reach the grain boundaries through hopping [57] and 'pile-up' at the grain boundaries if the grain boundaries' resistance is high enough and, hence, produce induced polarisation. In ferrites, the polarisation is a similar process to that of the conduction process. The free electrons in a dielectric medium need a finite time to line up their axes in the



direction of the applied field. If the frequency of the applied field is increased, free electrons cannot align with the applied field at a certain point and hence cannot follow the changes in the applied field over a certain frequency range [58]. As a result, the probability of free electrons reaching grain boundaries is decreased and the free electron polarisation virtually does not contribute to the polarisation that decreases the dielectric constant [56, 59]. At 1 MHz and above, all of the X ferrites have similar permittivity values of ~10-12.

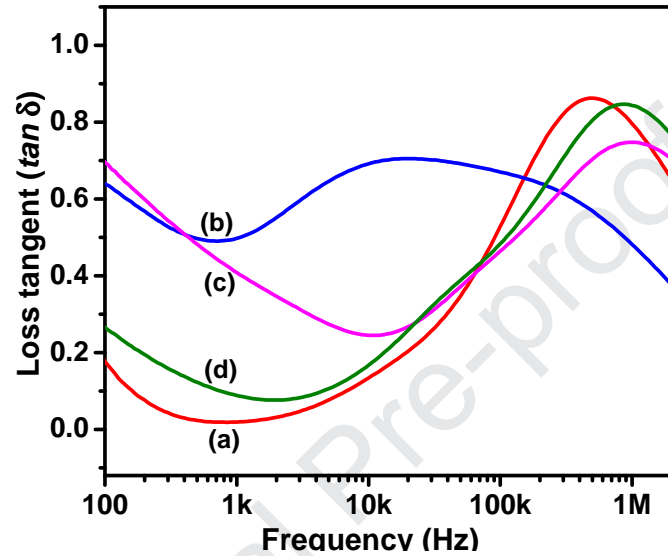


**Fig. 10.** Variation in loss tangent ( $\tan \delta$ ) as a function of frequency for  $\text{Ba}_2\text{Zn}_2\text{Fe}_{28}\text{O}_{46}$  hexaferrite samples heated at  $900^\circ\text{C}$  for 5 h., prepared with the different weight ratio of ginger root extract: (a) Sample (A), (b) Sample (B), (c) Sample (C), (d) Sample (D).

Fig.10 shows the variation of loss tangent ( $\tan \delta$ ) of all the prepared samples (Sample (A-D)) with frequency at room temperature. The value of loss tangent depends on different factors such as  $\text{Fe}^{+2}$  content, structural homogeneity, stoichiometry ratio, preparation time and heating temperature [60]. The value of loss tangent decreases with increasing frequency, that is because beyond a certain frequency limit hopping frequency of charge between  $\text{Fe}^{3+}$  and  $\text{Fe}^{2+}$  cannot follow the frequency of the applied electric field. The sample prepared with 35 g ginger root extract (Sample (B)) shows a broad resonance peak between 10 kHz to 100 kHz, while other samples show resonance between 500 kHz to 1 MHz frequency range.

AC conductivity ( $\sigma_{\text{ac}}$ ) of the samples was calculated by the formula [61];

$$\sigma_{\text{ac}} = 2\pi f \epsilon_0 \epsilon'' \quad (6)$$

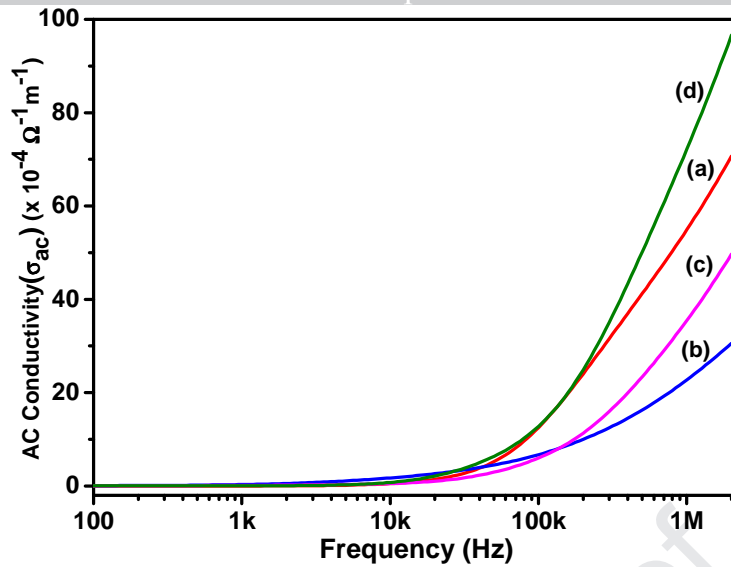


**Fig. 11.** AC conductivity of  $\text{Ba}_2\text{Zn}_2\text{Fe}_{28}\text{O}_{46}$  hexaferrite samples heated at  $900\text{ }^\circ\text{C}$  for 5 h., prepared with the different weight ratio of *ginger* root extract: (a) Sample (A), (b) Sample (B), (c) Sample (C), (d) Sample (D).

The variation of ac conductivity of all the hexaferrite samples (Sample (A-D)) with frequency (100 Hz - 2 MHz) at room temperature is shown in Fig. 11. It can be observed that ac conductivity increases with the increase of frequency, which is because increment in frequency increases the hopping frequency of the charge carriers between  $\text{Fe}^{2+}$  and  $\text{Fe}^{3+}$ .

### 3.5.1 Frequency-dependent impedance

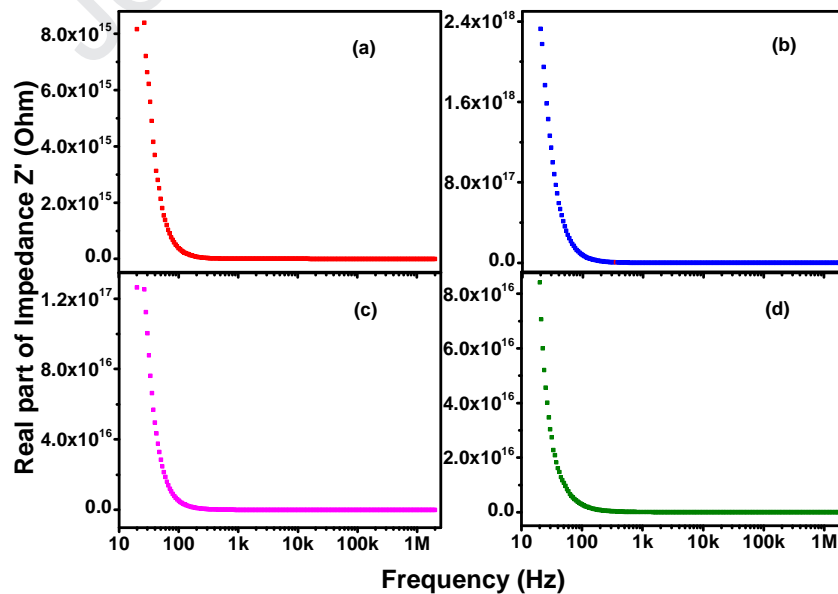


**Fig. 12.** Variation of the real part of impedance ( $Z'$ ) with frequency for X-type  $\text{Ba}_2\text{Zn}_2\text{Fe}_{28}\text{O}_{46}$  hexaferrite samples heated at  $900\text{ }^\circ\text{C}$  for 5 h., prepared with the different weight ratio of *ginger* root extract: (a) Sample (A), (b) Sample (B), (c) Sample (C), (d) Sample (D).

The real part of impedance ( $Z'$ ) and complex part of impedance ( $Z''$ ) as a function of applied field frequency in the range of 10 Hz to 2 MHz for X-type,  $\text{Ba}_2\text{Zn}_2\text{Fe}_{28}\text{O}_{46}$  hexaferrite samples heated at  $900\text{ }^\circ\text{C}$  for 5 h. measured at room temperature are shown in Fig. 12 and Fig. 13 respectively.

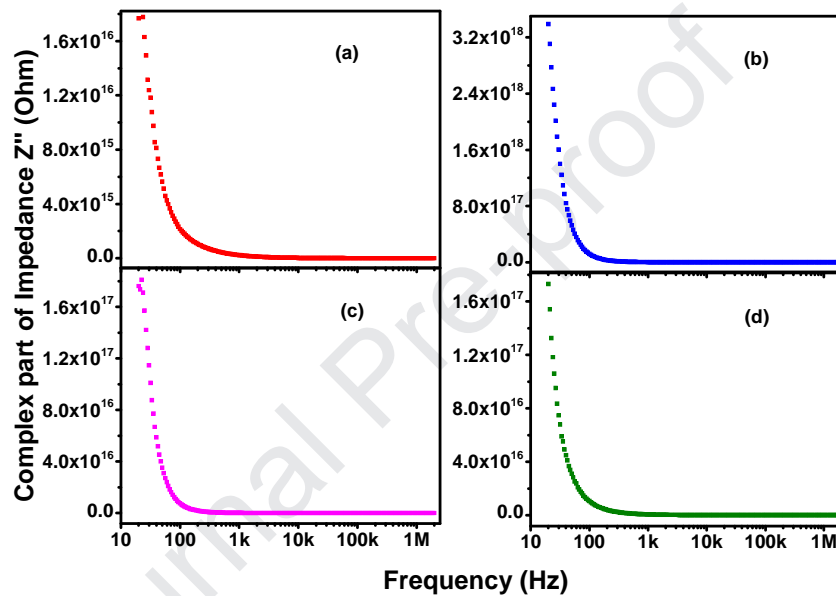
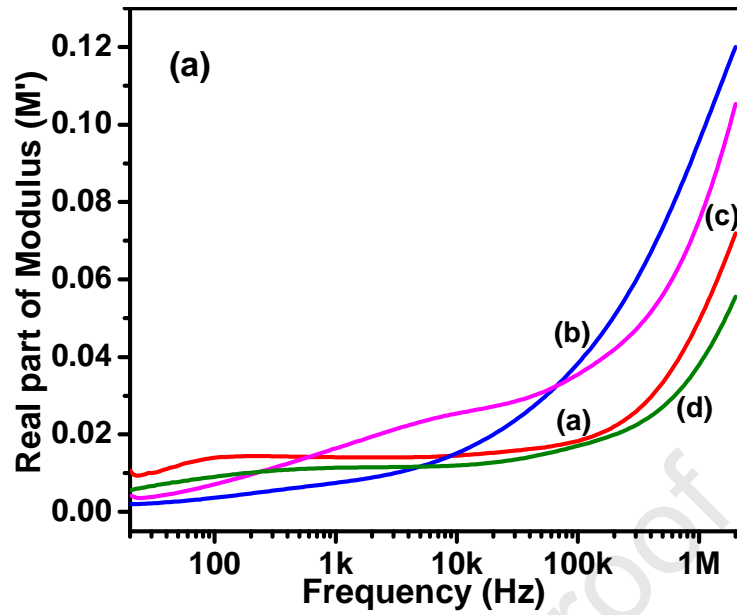


**Fig. 13.** Variation of the complex part of impedance ( $Z''$ ) with frequency for X-type,  $\text{Ba}_2\text{Zn}_2\text{Fe}_{28}\text{O}_{46}$  samples heated at  $900\text{ }^\circ\text{C}$  for 5 h., prepared with the different weight ratio of *ginger* root extract: (a) Sample (A), (b) Sample (B), (c) Sample (C), (d) Sample (D).

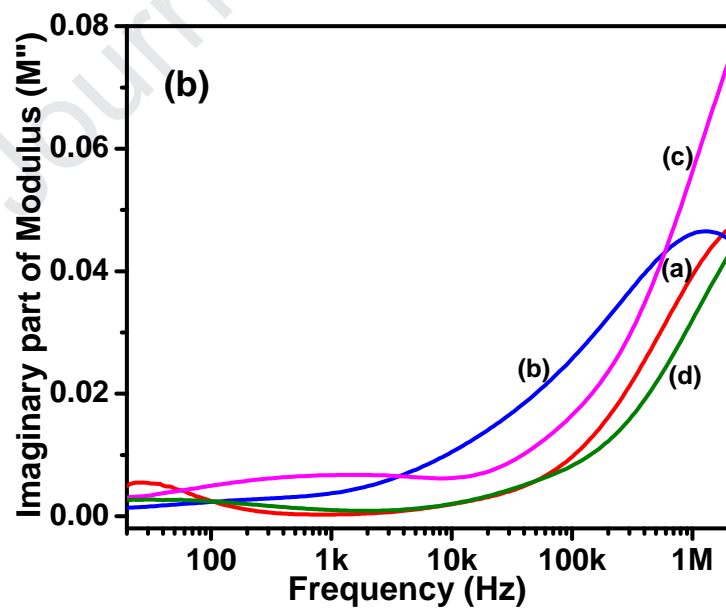
It can be seen from Fig. 12 and Fig. 13 that the real part of impedance ( $Z'$ ) and complex part of impedance ( $Z''$ ) for all different weight ratios of *ginger* root extract decreases fast as frequency increases. Their values become almost constant beyond 300 Hz frequency and approach to nearly zero, that shows no dependency of  $Z'$  and  $Z''$  on frequency.

### 3.5.2 Electric Modulus analysis

Analysis of electric modulus is important to understand the various parameters of electrical transport performance such as the rate of ion hopping and conductivity relaxation time contribution to the conductivity of the prepared hexaferrite material [62].



**Fig. 14 (a).** Variation in the real part of electric modulus as a function of frequency for  $\text{Ba}_2\text{Zn}_2\text{Fe}_{28}\text{O}_{46}$  hexaferrite samples heated at  $900\text{ }^\circ\text{C}$  for 5 h., prepared with the different weight ratio of *ginger* root extract: (a) Sample (A), (b) Sample (B), (c) Sample (C), (d) Sample (D).



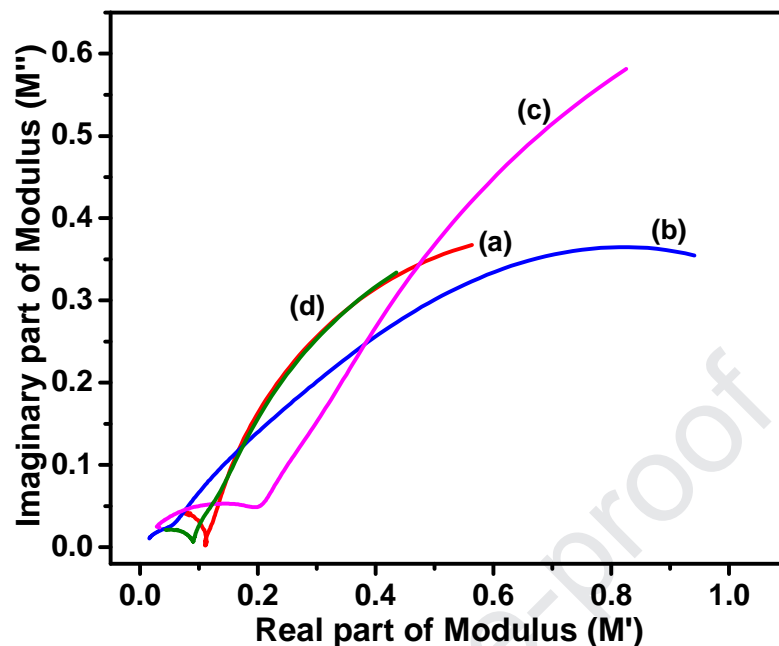
**Fig. 14 (b).** Variation in the imaginary part of electric modulus as a function of frequency for  $\text{Ba}_2\text{Zn}_2\text{Fe}_{28}\text{O}_{46}$  hexaferrite samples heated at  $900\text{ }^\circ\text{C}$  for 5 h., prepared with the different weight ratio of *ginger* root extract: (a) Sample (A), (b) Sample (B), (c) Sample (C), (d) Sample (D).

Fig. 14 (a) shows the variation of the real part of the electric modulus ( $M'$ ) of samples heated at 900 °C as a function of frequency. It can be observed from Fig. 14 (a) that at low frequency, the value of real electric modulus ( $M'$ ) of all samples prepared in presence of ginger root extract (Sample (A-D)) is low and at the high-frequency region, it increases very fast. When the electric field is applied, it decreases the restoring force between the charge carriers, which is responsible for the high value of  $M'$  at the high-frequency region [63]. The maximum value of real modulus ( $M' \sim 0.12$  at 2 MHz) is observed in the sample prepared with 35.0 g *ginger* extract.

The imaginary part of the electric modulus ( $M''$ ) for all samples heated at 900 °C (Sample (A-D)) is shown in Fig. 14 (b). The present graph explains the brief information about the charge transport mechanism, such as ion dynamics, conductivity relaxation and electrical transport mechanism as a function of the frequency [62]. The maximum value ( $M'' \sim 0.075$  at 2 MHz) is observed in the sample prepared with 52.5 g ginger root extract (Sample (C)). The relaxation peak is observed around 1 MHz in the sample prepared with 35.0 g *ginger* root extract (Sample (B)) due to the mobility of charge carriers. Below the relaxation peak, the charge carriers are mobile and above the relaxation peak, the charge carriers are immobile, which confined to a potential well [64].

Cole-Cole type plots provide information about the grains, grains boundary effects; are plotted and shown in Fig. 15. The Cole-Cole plot type (Nyquist plot) of electric modulus analysis is more helpful than impedance analysis ( $Z''$  versus  $Z'$ ). This analysis accurately separates the relaxation effects from grain and grain boundary in ferrite material. The imaginary part of impedance ( $Z''$ ) gives the relaxation dynamics from largest resistance of the material, while, the imaginary part of the modulus ( $M''$ ) gives the smallest capacitance (i.e. the highly conductive part) of the material [65]. It can be observed from Fig. 15 that all samples (Sample (A-D)) show semicircle arc in the low-frequency region attributed to the grain resistance [66]. The sample prepared with 52.5 g ginger root extract shows semicircle at the low-frequency region, that indicates the relaxation phenomena with different relaxation time ( $\tau$ ), associated with each relaxation. The capacitance values can be calculated at the maximum frequency ( $f_{\max}$ ) using the following relation [67]:

$$M'' = (\epsilon_0/2C) \quad (7)$$



**Fig. 15.** Cole-Cole type plots of  $\text{Ba}_2\text{Zn}_2\text{Fe}_{28}\text{O}_{46}$  hexaferrite samples heated at  $900\text{ }^\circ\text{C}$  for 5 h., prepared with the different weight ratio of *ginger* root extract: : (a) Sample (A), (b) Sample (B), (c) Sample (C), (d) Sample (D).

## Conclusions

X-type Barium zinc hexaferrite  $\text{Ba}_2\text{Zn}_2\text{Fe}_{28}\text{O}_{46}$  powder has been successfully synthesized using the combustion treatment method at  $900\text{ }^\circ\text{C}$  for 5 h. in presence of different weight ratios of *ginger* root. From XRD analysis it has been found that the sample with 52.5 g *ginger* root, heated at  $900\text{ }^\circ\text{C}$  contained less impurity of hematite peak (17.39 %) compared to other samples heated at  $900\text{ }^\circ\text{C}$ . The sample prepared with 52.5 g *ginger* root extract possesses the highest value of saturation magnetization ( $M_S = 33.87\text{ Am}^2\text{ kg}^{-1}$ ) in comparison with the other prepared samples, and all were hard ferrites. At low frequencies ( $>2\text{ MHz}$ ), relative permittivity was constant between 5 and 12 above 800 kHz.

## Acknowledgments

This work was supported by DRS–SAP (Phase-II, F-530/17/DRS-II/2018 (SAP-I)) grant, New Delhi, India and DST–FIST (level- I, No. SR/FST/PSI-198/2014) grant, India. One of the authors (Amrin R. Kagdi) acknowledges the Ministry of Minority Affairs, Govt.

of India for providing Maulana Azad National Fellowship (No. F1-17.1/2013-14/MANF-2013-14-MUS-GUJ-28541). R. C. Pullar wishes to thank National funding provided by FCT (Fundação para a Ciência e a Tecnologia, Portugal) grant IF/00681/2015, and this work was developed within the scope of the project CICECO-Aveiro Institute of Materials, UIDB/50011/2020 & UIDP/50011/2020, financed by national funds through the Foundation for Science and Technology/MCTES. K. M. Batoo is thankful for the deanship of scientific research at King Saud University, Rihadh, Saudi Arabia, under the project code No. RG 1437-030 and thankful to the Researchers Supporting project (RSP-2019/148) at King Saud University for financial support.

## References

- [1] S. Malhotra, M. Chitkara, I. S. Sandhu, Naini Dawar, J. Singh, Investigation of Structural, Magnetic and Dielectric Properties of Terbium Doped Strontium Hexaferrite for High Frequency Applications, *Ind. J. Sci. Techn.* 9 (2016) 96638.
- [2] R. C. Pullar, Hexagonal Ferrites a review of the synthesis, properties and applications of hexaferrite ceramics, *Prog. Mater. Sci.* 57 (2012) 1191-1334
- [3] Leslie-Pelecky D L, Rieke R D. Magnetic properties of nanostructured materials, *Chem Mater.* 8 (1996) 1770-1783.
- [4] F. J. Himpsel, J. E. Ortega, G. J. Mankey, R.F. Willis, *Magnetic nanostructures*, *Adv. Phys.* 47 (1998) 511-597.
- [5] M. Sugimoto, The past, present and future of ferrites, *J. Am. Ceram. Soc.* 82 (1999) 269-280.
- [6] G. Bate, Magnetic recording materials since 1975, *J. Magn. Magn. Mater.* 100 (1991) 413-424.
- [7] A. Jordan, R. Scholz, P. Wust, H. Schirra, T. Schiestel, H. Schmidt, R. Felix, Endocytosis of dextran and silan-coated magnetite nanoparticles and the effect of intracellular hyperthermia on human mammary carcinoma cells in vitro, *J Magn. Magn. Mater.* 194 (1999) 185-196.
- [8] D. H. Kim, D. E. Nikles, D. T. Johnson, C.S. Brazel, Heat generation of aqueously dispersed  $\text{CoFe}_2\text{O}_4$  nanoparticles as heating agents for magnetically activated drug delivery and hyperthermia, *J. Magn. Magn. Mater.* 320 (2008) 2390-2396.
- [9] S. Mornet, S. Vasseur, F. Grasset, E. Duguet, Magnetic nanoparticle design for medical diagnosis and therapy, *J. Mater. Chem.* 14 (2004) 2161-2175.

- [10] S. Wada, K. Tazawa, I. Furuta, H. Nagae, Antitumor effect of new local hyperthermia using dextran magnetite complex in hamster tongue carcinoma, *Oral Dis* 9 (2003) 218-223.
- [11] M. D. Shultz, S. Calvin, P. P. Fatouros, S. A. Morrison, E. E. Carpenter, *Enhanced ferrite nanoparticles as MRI contrast agents*, *J. Magn. Magn. Mater.* 311 (2007) 464-468.
- [12] L. Zhen, K. He, C. Y. Xu, W. Z. Shao, Synthesis and characterization of single crystalline  $\text{MnFe}_2\text{O}_4$  nanorods via a surfactant-free hydrothermal route, *J. Magn. Magn. Mater.* 320 (2008) 2672-2675.
- [13] S.R. Pezeshki, M.W. Hester, Q. Lin, J.A. Nyman, *The effects of oil spill and clean-up on dominant US Gulf coast marsh macrophytes: a review*, *Environ. Pollut.* 108 (2000) 129-139.
- [14] J.A. Dahl, B.L.S. Maddux, J.E. Hutchison, *Toward Greener Nanosynthesis*, *Chem. Rev.* 107 (2007) 2228-2269.
- [15] M. Sastry, A. Ahmad, M.I. Khan, R. Kumar, C.M. Niemeyer, C.A. Mirkin (Eds.), *Microbial Nanoparticle Production*, Wiley-VCH, Weinheim, Germany, (2004) 126-135.
- [16] A. Chakraborty, D.K. Das, M. Sinha, S. Dey, S. Bhattacharjee, Moringa oleifera leaf extract mediated green synthesis of stabilized gold nanoparticles *J. Bionanosci.* 7 (2013) 415-419.
- [17] S. Sathya, S. Parthasarathi, V. Murugan, S. Ramesh, Y. Kyusik, Biogenic synthesis of multidimensional gold nanoparticles assisted by *Streptomyces hygroscopicus* and its electrochemical and antibacterial properties, *BioMetals* 25 (2012) 351-360.
- [18] G. Rishalan, P. Alisa, R.M. Gengan, K. Anand, A.A. Chuturgoon, Silver nanoparticles of *Albizia adianthifolia*: the induction of apoptosis in human lung carcinoma cell line, *J. Nanobiotechnol.* 11:5 (2013) 1-9.
- [19] B.V. Tirupanyam, Ch. Srinivas, S.S. Meena, S.M. Yusuf, A. Satish Kumar, D.L. Sastry, V. Seshubai, Investigation of structural and magnetic properties of co-precipitated Mn–Ni ferrite nanoparticles in the presence of  $\alpha\text{-Fe}_2\text{O}_3$  phase, *J. Magn. Magn. Mater.* 392 (2015) 101–106.
- [20] P. Kaur, S.K. Chawla, S.S. Meena, S.M. Yusuf, K. Pubby, S. B. Narang, Synthesis of Co-Zr Doped Nanocrystalline Strontium Hexaferrites by Sol–Gel Auto-Combustion Route Using Sucrose as Fuel and Study of their Structural, Magnetic and Electrical Properties, *Ceram. Int.* 43 (2017) 590–598.



- [21] S. K. Chawla, R. K. Mudsainiyan, S. S. Meena, S. M. Yusuf, Sol-gel synthesis, structural and magnetic properties of nanoscale M-type barium hexaferrites  $\text{BaCo}_x\text{Zr}_x\text{Fe}_{(12-2x)}\text{O}_{19}$ , *J. Magn. Magn. Mater.* 350 (2014) 23–29.
- [22] M. Hashim, S.E. Shirsath, S.S. Meena, M.L. Mane, S. Kumar, P. Bhatt, R. Kumar, N.K. Prasad, S.K. Alla, J. Shah, R.K. Kotnala, K.A. Mohammed, E. Senturk, Alimuddin, Manganese ferrite prepared using reverse micelle process: Structural and magnetic properties characterization, *J. Alloys Compd.* 642 (2015) 70–77.
- [23] J. Singh, C. Singh, D. Kaur, H. Zaki, I.A. Abdel-Latif, S. BindraNarang, R. Jotania, S.R. Mishra, R. Joshi, P. Dhruv, M. Ghimire, S.E. Shirsath, S.S. Meena, Elucidation of phase evolution, microstructural, Mossbauer and magnetic properties of Co 2p eAl 3p doped M-type BaSr hexaferrites synthesized by a ceramic method, *J. Alloys Compd.* 695 (2017) 1112–1121.
- [24] S. C. Bhargava, H. Kunkel, S. Singh, A. H. Morrish, Z. W. Li, Spin glass ordering of  $\text{Zn}_{0.75}\text{Co}_{0.25}\text{Fe}_{0.5}\text{Cr}_{1.5}\text{O}_4$  cubic spinel, *Sol. Stat. Comm.* 126 (2003) 535–540.
- [25] V. Parashar, R. Prashar, B. Sharma, A. C. Pandey, Parthenium leaf extract mediated synthesis of silver nanoparticles: a novel approach towards weed utilization, *Dig. J. Nanomater. Biostruct.* 4 (2009) 45-50.
- [26] N. Saifuddin, C. W. Wong, A. A. Nuryusumina, Rapid biosynthesis of silver nanoparticles using culture supernatant of bacteria with microwave irradiation. *J. Chem.* 6 (2009) 61-70.
- [27] K. C. Bhansa, S. F. D Souza, Extracellular biosynthesis of silver nanoparticles using the fungus *Aspergillus fumigates*. *Colloids and Surfaces B: Biointerfaces.* 47 (2006) 160-164.
- [28] K. Chaieb, H. Hajlaoui, T. Zmantar, A.B. Kahla-Nakbi, M. Rouabhia, K. Mahdouani, A. Bakhruf, The chemical composition and biological activity of clove essential oil, *eugenia caryophyllata* (*syzigium aromaticum* L. Myrtaceae): a short review, *Phyther. Res.* 21 (2007) 501–506
- [29] S.T. Chang, P.F. Chen, S.C. Chang, Antibacterial activity of leaf essential oil and their constituents from *Cinnamomum osmophloeum*, *J. Ethnopharmacol.* 77 (2001) 123–127.
- [30] H.K. Kwon, W.K. Jeon, J.S. Hwang, C.G. Lee, J.S. So, J.A. Park, et al., Cinnamon extract suppresses tumor progression by modulating angiogenesis and the effector function of CD8+T cells, *Cancer Lett.* 278 (2009) 174–182.
- [31] B.H. Ali, G. Blunden, M. O. Tanira, A. Nemmar, Some phytochemical, pharmacological and toxicological properties of ginger (*Zingiber officinale* Roscoe): A review of recent research, *Food. Chem. Toxicol.* 46 (2008) 409–420.

- [32] A.M. Bode, Z. Dong, *The Amazing and Mighty Ginger*, Herbal Medicine: Biomolecular and Clinical Aspects. 2nd edition, CRC Press, Taylor & Francis; (2011).
- [33] I.T. Carvalho, L. Santos, Antibiotics in the aquatic environments: A review of the European scenario, *Environ. Intern.* 94 (2016)736–757.
- [34] Y. Sakai, H. Nagase, Y. Ose, T. Sato, M. Kawai, M. Mizuno, Effects of medicinal plant extracts from Chinese herbal medicines on the mutagenic activity of benzo(a)pyrene, *Mutat. Res.* 206 (1988) 327–334.
- [35] A. H. Rahmani, F. M. Al. Shabrmi, S. M. Aly, Active ingredients of ginger as potential candidates in the prevention and treatment of diseases via modulation of biological activities, *Int. J. Phys. Pathophy. Pharma.* 6 (2014) 125–136.
- [36] P.R. Shirin Adel, J. Prakash, Chemical composition and antioxidant properties of ginger root (*Zingiber officinale*), *J. Medic. Plant. Res.* 4 (2010) 2674–2679.
- [37] F. Tavakoli, M. Salavati-Niasari, F. Mohandes, Green synthesis and characterization of graphene nanosheets, *Mater. Res. Bull.* 63 (2015) 51–57.
- [38] F. Tavakoli, M. Salavati-Niasari, F. Mohandes, Green synthesis of flower-like CuI microstructures composed of trigonal nanostructures using pomegranate juice, *Mater. Lett.* 100 (2013) 133–136.
- [39] G. Yen, P. Duh, C. Tsai, Relationship between antioxidant activity and maturity of peanut hulls. *J. Agric. Food Chem.* 41 (1993) 67–70.
- [40] P. Siddhuraju, P. Mohan, K. Becker, Studies on the antioxidant activity of Indian Laburnum (*Cassia fistula* L.): A preliminary assessment of crude extracts from stem bark, leaves, flowers and fruit pulp. *Food Chem.* 79(2002) 61–67.
- [41] N. Turkmen, F. Sari, Y. Velioglu, Effects of extraction solvents on concentration and antioxidant activity of black and black mate tea polyphenols determined by ferrous tartrate and Folin-Ciocalteu methods, *Food Chem.* 99 (2006) 835–841.
- [42] X. Huang, J. Zhang, L. Wang, Q. Zhang, Simple and reproducible preparation of barium hexagonal ferrite by adsorbent combustion method, *J. Alloys Compd.* 540 (2012) 137–140.
- [43] S. K. Chawla, R. K. Mudsainiyan, S. S. Meena, S. M. Yusuf, Sol–gel synthesis, structural and magnetic properties of nanoscale M-type barium hexaferrites  $\text{BaCo}_x\text{Zr}_x\text{Fe}_{(12-2x)}\text{O}_{19}$ , *J. Magn. Magn. Mater.* 350 (2014) 23–29.
- [44] M. K. Raju, FT-IR studies of Cu substituted Ni-Zn ferrites for structural and vibrational investigations, *Chem. Sci. Trans.* 2015 4(1) (2015) 137–142.
- [45] I. Sadiq, I. Ali, E. Rebrov, S. Naseem, M. N. Ashiq, M.U. Rana, Nanosized Ce–Zn substituted microwave absorber material for X-band applications, *J. Magn. Magn. Mater.* 370 (2014) 25–31.

- [46] M.U.I Ali, M.S. Awan, M. Ahmad, M.A. Iqbal, Structural, Electrical, and Microstructure Properties of Nanostructured Calcium doped Ba-Hexaferrites Synthesized by Sol-Gel Method, *J. Supercond. Nov. Magn.* 26 (2013), 3277–3286.
- [47] M. Ahmad, R. Grössinger, M. Kriegisch, F. Kubel, M.U. Rana, Magnetic and microwave attenuation behavior of Al-substituted  $\text{Co}_2\text{W}$  hexaferrites synthesized by sol-gel autocombustion process, *J. Curr. Appl. Phys.* 12 (2012) 1413–1420.
- [48] M.J. Iqbal, M.N. Ashiq, I.H. Gul, Physical, electrical and dielectric properties of Ca-substituted strontium hexaferrite ( $\text{SrFe}_{12}\text{O}_{19}$ ) nanoparticles synthesized by coprecipitation method, *J. Magn. Magn. Mater.* 322 (2010) 1720–1726.
- [49] K.H.J. Buschow, F.R. de Boer, *Physics of Magnetism and Magnetic Materials*, Kluwer Academic Publishers, New York, Boston, Dordrecht, London, Moscow, (2004) 75–83.
- [50] B. X. Gu, Magnetic properties of  $\text{Ba}_2\text{Me}_2\text{Fe}_{28}\text{O}_{46}$  ( $\text{Me}_2\text{-X}$ ,  $\text{Me}=\text{Ni}$ ,  $\text{Cu}$ ,  $\text{Mg}$ , and  $\text{Zn}$ ) hexaferrites, *J. Appl. Phys.* 70 (1991) 372–375.
- [51] M. Tadic, D. Markovic, V. Spasojevic, V. Kusigerski, M. Remskar, J. Pirnat, Z. Jaglicic, Synthesis and magnetic properties of concentrated  $\alpha\text{-Fe}_2\text{O}_3$  nanoparticles in a silica matrix, *J. Alloys Compd.* 441 (2007) 291–296.
- [52] A. Nadar, A. M. Banerjee, M. R. Pai, R.V. Pai, S. S. Meena, R. Tewari, A.K. Tripathi, Catalytic properties of dispersed iron oxides  $\text{Fe}_2\text{O}_3/\text{MO}_2$  ( $\text{M} = \text{Zr}$ ,  $\text{Ce}$ ,  $\text{Ti}$  and  $\text{Si}$ ) for sulfuric acid decomposition reaction: Role of support, *Int. J. Hyd. Energy* 43 (2018) 37–52.
- [53] D. Ravinder, P.V. Bhaskar Reddy, P. Shalini, Frequency and composition dependence of dielectric behavior of copper substituted lithium ferrites, *J. Mater. Sci. Lett.* 22 (2003) 1599–1601.
- [54] M. M. Haque, M. Huq, M.A. Hakim, Densification, magnetic and dielectric behaviour of Cu-substituted Mg-Zn ferrites, *Mater. Chem. Phys.* 112 (2008) 580–586.
- [55] B. P. Rao, K.H. Rao, T. Vasantha, A. Paduraru, O.F. Caltun, DC resistivity and dielectric studies on  $\text{Ti}^{4+}$  substituted Ni-Zn ferrites, *J. Optoelectron Adv. M.* 7 (2005) 701–704.
- [56] C. G. Koops, On the dispersion of resistivity and dielectric constant of some semiconductors at audio frequencies, *J. Phys. Rev.* 83 (1951) 121–124.
- [57] A. Aharoni, *Introduction to the Theory of Ferromagnetism*, Clarendon Press, Oxford, 1996.
- [58] M. A. El Hiti, Dielectric behaviour in Mg-Zn ferrites, *J. Magn. Magn. Mater.* 192 (1999) 305–313.
- [59] J. C. Dyre, T. B. Schroder, Universality of ac conduction in disordered solids, *Rev. Mod. Phys.* 72 (2000) 873–892.

- [60] S. Dutta, R. N. P. Choudhry, P. K. Sinha, Impedance spectroscopy studies on Ga-ion-modified PLZT ceramics, *Phys. Status Solidi*. 202 (2005) 1172–1181.
- [61] N. Pandsa, S. Pattanayak, H.B.K. Sharma, R.N.P. Choudhary, Structural and electrical properties of BiFeO<sub>3</sub>–PbTiO<sub>3</sub> system, *J. Mater. Sci. Mater. Electron*. 26 (2015) 10012–10019.
- [62] S. R. Ejaz, M. A. Khan, M. F. Warsi, M.N. Akhtar, A. Hussain, Study of structural transformation and hysteresis behavior of Mg-Sr substituted X-type hexaferrites, *Ceram. Int.* 44 (2018) 18903–18912.
- [63] K. P. Padmasree, D.K. Kanchan, A.R. Kulkarni, Impedance and modulus studies of the solid electrolyte system 20CdI<sub>2</sub>-80 [xAg<sub>2</sub>O-y(0.7V<sub>2</sub>O<sub>5</sub>-0.3B<sub>2</sub>O<sub>3</sub>)], where 1≤x/y≤3, *Solid State Ion*. 177 (2006) 475–482.
- [64] S. M. Patange, S.E. Shirsath, K.S. Lohar, S.S. Jadhav, N. Kulkarni, K.M. Jadhav, Electrical and switching properties of NiAl<sub>x</sub>Fe<sub>2-x</sub>O<sub>4</sub> ferrites synthesized by chemical method, *Phys. B: Condens. Mater.* 406 (2011) 663–668.
- [65] R. N. Bhowmik, I. P. Muthuselvam, Dielectric properties of magnetic grains in CoFe<sub>1.95</sub>Ho<sub>0.05</sub>O<sub>4</sub> spinel ferrite, *J. Magn. Magn. Mater.* 335 (2013) 64–74.
- [66] Y. Bai, J. Zhou, Z. Gui, L. Li, Electrical properties of non-stoichiometric Y- type hexagonal ferrite, *J. Magn. Magn. Mater.* 278 (2004) 208–213.
- [67] S. Narayanan, A. K. Baral, V. Thangadurai, Dielectric characteristics of fast Li ion conducting garnet-type Li<sub>5+2x</sub>La<sub>3</sub>Nb<sub>2-x</sub>Y<sub>x</sub>O<sub>12</sub> (x = 0.25, 0.5 and 0.75), *Phys. Chem. Chem. Phys.* 18 (2016) 15418–15426.

## Highlights of the work

- The effect of the different amounts of ginger root extract on phase formation, as well as on magnetic and dielectric properties of  $\text{Ba}_2\text{Zn}_2\text{Fe}_{28}\text{O}_{46}$  has been investigated.
- Barium-zinc hexaferrite (along with some hematite) has been formed at 900 °C by using *ginger* extract as a reducing agent in reactions.
- Prepared X-ferrites were hard magnets, with coercivity values ( $H_c$ ) between 108-157  $\text{kA m}^{-1}$ , and squareness ratios  $> 0.5$ .
- 52.5 g *ginger* root gave the highest saturation magnetisation ( $33.87 \text{ Am}^2 \text{ kg}^{-1}$ ), showing it to be a useful natural plant extract as a reducing fuel for the low temperature synthesis of X-ferrites.
- 35 g ginger gave a broad resonance peak at 10 kHz - 100 kHz, while others showed resonance at 500 kHz - 1 MHz.
- Low frequency relative permittivity was between 5-12 at 800 kHz – 2 MHz for all X ferrites.

**Declaration of interest**

The authors declare that they have not known to competing financial interest or personal relationship that could appeared to influence to work reported to this paper.

Amrin Kagdi, Robert C. Pullar, Sher Singh Meena, Rajshree B. Jotania, Khalid Mujasam  
Battoo

Journal Pre-proof